Acta Mechanica Sinica
https://doi.org/10.1007/s10409-020-01017-3

RESEARCH PAPER

A theory of mechanobiological sensation: strain amplification/attenuation of coated liquid inclusion with surface tension

Fei Ti[1] · Xin Chen[2,3,4] · Haiqian Yang[4] · Shaobao Liu[1] · Tian Jian Lu[1,3,4]

Received: 15 August 2020 / Revised: 25 September 2020 / Accepted: 25 October 2020

Abstract
Cells are compressible and can be regarded as a kind of coated liquid inclusion embedded in a three-dimensional elastic matrix. In the presence of far-field loading, how the coating influences the mechanical response (e.g., volume change) of the liquid inclusion remains elusive, especially when surface tension effects become significant at cell size level. We developed a theoretical model to characterize the mechanical amplification or attenuation role of coating on spherical liquid inclusions, with surface tension and liquid compressibility accounted for. We found that surface tension could increase the volumetric strain of the inclusion through decreasing its effective bulk modulus. We further found that, when there is a monotonic stiffness variation (either decreasing or increasing) from matrix via coating to inclusion, the presence of coating amplified the volumetric strain compared with the case without coating; in the opposite, when there is a non-monotonic stiffness change from matrix via coating to inclusion, the volumetric strain is attenuated by the coating. The results are useful for understanding and exploring the mechanobiological sensation of certain types of cell, e.g., osteocytes and cancer cells.

Keywords Surface tension · Liquid inclusion · Mechanobiological sensation · Cancer cell

1 Introduction

Cells can be regarded as a kind of coated compressible liquid inclusions in biological bodies [1–3], with the coating regulating the physiological function of the cell when it receives mechanical signals from cellular microenvironment [4, 5]. For instance, osteocyte cell is surrounded by a coating of pericellular matrix (PCM), which tends to amplify mechanical signals from cellular microenvironment [6, 7]. For cancer cell, the abnormal deposition and remodeling of extracellular matrix (ECM) leads to increased stiffness of the ECM that forms a coating on cell surface [8]. The stiffened coating can affect (e.g., attenuate) mechanical signal transduction, thus crucially influencing the rate and direction of tumor cell migration [9].

The classical model of a single solid inclusion in an infinite elastic matrix subject to far field loadings was developed by Eshelby [10], which was extended by Walpole [11] to a coated inclusion. The Biot model and its various extensions have been extensively employed to analyze stress concentration around an inclusion [12–14], predict the homogenized (effective) properties (elastic moduli, thermal/electrical con-

Executive Editor: Xi-Qiao Feng.

Electronic supplementary material The online version of this article (https://doi.org/10.1007/s10409-020-01017-3) contains supplementary material, which is available to authorized users.

✉ Shaobao Liu
sbliu@nuaa.edu.cn

✉ Tian Jian Lu
tjlu@nuaa.edu.cn

1 State Key Laboratory of Mechanics and Control of Mechanical Structures, Nanjing University of Aeronautics and Astronautics, Nanjing 210016, China

2 Xi'an Modern Chemistry Research Institute, Xi'an 710065, China

3 State Key Laboratory for Strength and Vibration of Mechanical Structures, Xi'an Jiaotong University, Xi'an 710049, China

4 Bioinspired Engineering & Biomechanics Center (BEBC), Xi'an Jiaotong University, Xi'an 710049, China

Published online: 07 January 2021

ductivity, etc.) of a composite with coated inclusions [15–18], and design materials with inhomogeneous microstructures for specific applications [19–21]. Further, built upon the model of coated solid inclusion, a variety of generalized self-consistent methods were proposed to predict the effective properties of particulate composites or nanocomposites with high concentration of inclusions [22–26]. For example, Mancarella et al. [27] used this approach to predict the influence of surface tension on the effective moduli of composites embedded with incompressible liquid inclusions, while Chen et al. [3] quantified the effect of liquid compressibility on the morphology evolution of a liquid inclusion under external loading. Further, in the absence of surface tension, Chen et al. [28] studied the amplification and attenuation of mechanical fields in healthy and diseased tissues using the model of coated liquid inclusion. However, the effect of coating and liquid compressibility on the inclusion response and, in particular, the role of surface tension in strain amplification/attenuation need to be further investigated.

In the current study, built upon the coated liquid inclusion model of Chen et al. [28], we propose a mechanical model to describe the response of coated compressible liquid inclusions with surface tension. We focus on how the mechanical properties (e.g., stiffness and thickness) of the coating, liquid compressibility and surface tension influence the volumetric strain of the liquid inclusion. According to the theoretical results, the phenomenon of strain amplification/attenuation by coated inclusions (e.g., osteocytes and cancer cell) is discussed.

2 Problem statement

Consider a single spherical liquid inclusion coated with a solid coating embedded in an infinite matrix (Fig. 1). The inclusion and coating have a radius of R_i and R_c, respectively. Both the coating and the matrix are assumed to be linear elastic. Let the shear modulus and Poisson ratio be denoted as G_a (N·m^{-2}) and ν_a, with $a = c$ for coating and $a = m$ for matrix. With the initial pressure of the liquid balanced by surface tension, the matrix is free of stress before far field loading is applied.

The governing equations (e.g., geometric, physical and equilibrium equations) for the matrix are:

$$\boldsymbol{\varepsilon}^{(m)} = \frac{1}{2}\left(\nabla \mathbf{u}^{(m)} + \mathbf{u}^{(m)}\nabla\right), \tag{1a}$$

$$\boldsymbol{\sigma}^{(m)} = 2G_m\left[\frac{\nu_m}{1-2\nu_m}\mathrm{tr}\left(\boldsymbol{\varepsilon}^{(m)}\right) + \boldsymbol{\varepsilon}^{(m)}\right], \tag{1b}$$

$$\nabla \cdot \boldsymbol{\sigma}^{(m)} = 0, \tag{1c}$$

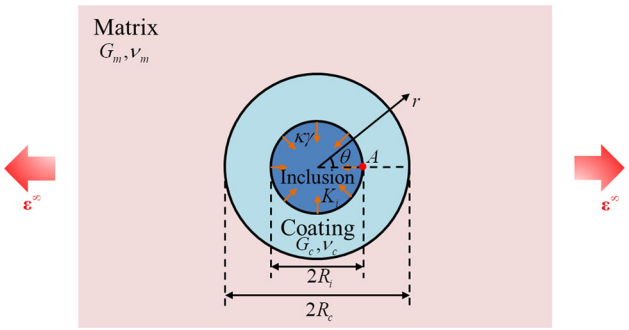

Fig. 1 Schematic diagram of a coated liquid inclusion. The spherical liquid inclusion is coated by a spherical coating, and the outside of the coating is an infinite matrix. The radius of the inclusion and coating are R_i and R_c respectively. The bulk modulus of the liquid inclusion is K_i, and the shear modulus and Poisson's ratio of the coating and matrix are G_c, ν_c and G_m, ν_m respectively. There is surface tension $\kappa\gamma$ at the interface between the inclusion and the coating, where κ is the surface curvature of the interface, γ is the surface energy density. There exists a far-field strain ε^∞ at infinity of the matrix

where $\mathbf{u}^{(m)}$, $\boldsymbol{\varepsilon}^{(m)}$ and $\boldsymbol{\sigma}^{(m)}$ are the displacement, strain and stress tensors in the matrix, respectively. Similarly, the governing equations for the coating are:

$$\boldsymbol{\varepsilon}^{(c)} = \frac{1}{2}\left(\nabla \mathbf{u}^{(c)} + \mathbf{u}^{(c)}\nabla\right), \tag{2a}$$

$$\boldsymbol{\sigma}^{(c)} = 2G_c\left[\frac{\nu_c}{1-2\nu_c}\mathrm{tr}\left(\boldsymbol{\varepsilon}^{(c)}\right) + \boldsymbol{\varepsilon}^{(c)}\right], \tag{2b}$$

$$\nabla \cdot \boldsymbol{\sigma}^{(c)} = 0, \tag{2c}$$

where $\mathbf{u}^{(c)}$, $\boldsymbol{\varepsilon}^{(c)}$ and $\boldsymbol{\sigma}^{(c)}$ are the displacement, strain and stress tensors in the coating.

Let the liquid be linearly compressible [29], namely:

$$K_i \frac{\Delta V}{V_0} = -p, \tag{3}$$

where K_i (N·m^{-2}) is the bulk modulus of the liquid, V_0 and ΔV are the initial volume and volumetric change of the liquid inclusion, and p is the liquid pressure after far field loading is applied.

In the far field, a uniform strain $\boldsymbol{\varepsilon}^\infty$ is applied, as:

$$\boldsymbol{\varepsilon}^{(m)}\Big|_{|\mathbf{x}|\to\infty} = \boldsymbol{\varepsilon}^\infty. \tag{4}$$

To solve the problem of Fig. 1, it is necessary to choose the form of far field loading in Eq. (4). In general, three types of far field loading can be selected: uniaxial loading (stretch and compression), simple shear, and radial loading (i.e., hydrostatic loading). On one hand, only the solution obtained under uniaxial loading can be used to derive solutions for the other two loading types. On the other hand, focus of the present study is placed upon the mechanical states of the inclusion.

For a liquid inclusion, the most important mechanical states are its volumetric strain and pressure, and only uniaxial loading and radial loading at far field can change such states. Therefore, solution of the problem is derived only under uniaxial loading so that the far field strain $\boldsymbol{\varepsilon}^{\infty}$ can be written in the Cartesian coordinate system, as:

$$\boldsymbol{\varepsilon}^{\infty} = \begin{pmatrix} \varepsilon^{\infty} & 0 & 0 \\ 0 & -\nu_m \varepsilon^{\infty} & 0 \\ 0 & 0 & -\nu_m \varepsilon^{\infty} \end{pmatrix}. \tag{5}$$

At the interface between the inclusion and its coating, the surface tension is assumed to be in equilibrium with the initial liquid pressure in the absence of far field loading. Force equilibrium then dictates:

$$p_0 \mathbf{n}_0 = \gamma \kappa_0 \mathbf{n}_0, \tag{6}$$

where p_0 is the initial liquid pressure of the liquid inclusion, $\mathbf{n}_0$ is the initial normal vector of the liquid-coating interface, γ is an isotropic and strain-independent surface tension, and κ_0 is the initial surface curvature.

When there is a load in the far field, force equilibrium dictates:

$$\boldsymbol{\sigma}^{(c)} \cdot \mathbf{n}_1 = -(p + p_0)\mathbf{n}_1 + \gamma \kappa \mathbf{n}_1, \tag{7}$$

where $\mathbf{n}_1$ is the normal vector of the liquid-coating interface after loading, and κ is the surface curvature after loading. For a spherical liquid inclusion of radius R, the surface normal vector $\mathbf{n}_1$ and curvature κ can be expressed as [30]:

$$n_1 = \left(1, \frac{u_\theta}{R} - \frac{1}{R}\frac{\partial u_r}{\partial \theta}, 0\right), \tag{8}$$

$$\kappa = \frac{2}{R} - \frac{1}{R^2}\left(2u_r + \cot\theta \frac{\partial u_r}{\partial \theta} + \frac{\partial^2 u_r}{\partial \theta^2}\right). \tag{9}$$

At the interface between the coating and the matrix, the force equilibrium is:

$$\boldsymbol{\sigma}^{(c)} \cdot \mathbf{n}_2 = \boldsymbol{\sigma}^{(m)} \cdot \mathbf{n}_2, \tag{10}$$

where $\mathbf{n}_2$ is the normal vector of the interface. In addition, the displacement field is assumed to be continuous across the coating-matrix interface such that:

$$\mathbf{u}^{(c)} = \mathbf{u}^{(m)}. \tag{11}$$

Here, $\mathbf{u}^{(c)}$ and $\mathbf{u}^{(m)}$ are the displacement of the coating and matrix, respectively.

3 Solution of the problem

3.1 Displacement and stress fields in the coating and matrix

Built upon our previous work [3], for the present problem of Fig. 1, the governing equations detailed in the previous section can be solved, leading to the following displacement fields in the coating and matrix:

$$u_r^{(a)} = B_1^{(a)} \varepsilon r + B_2^{(a)} \frac{R_i^3}{r^2} + \frac{3\cos(2\theta)+1}{4} \times \left[12\nu_i A_1^{(a)} \frac{r^3}{R_i^2} + 2A_2^{(a)} r + 2(5-4\nu_i) A_3^{(a)} \frac{R_i^3}{r^2} - 3A_4^{(a)} \frac{R_i^5}{r^4}\right], \tag{12a}$$

$$u_\theta^{(a)} = -\frac{3\sin(2\theta)}{2}\left[(7-4\nu_i) A_1^{(a)} \frac{r^3}{R_i^2} + A_2^{(a)} r + 2(1-2\nu_i) A_3^{(a)} \frac{R_i^3}{r^2} + A_4^{(a)} \frac{R_i^5}{r^4}\right], \tag{12b}$$

$$u_\phi^{(a)} = 0, \tag{12c}$$

where $a = c$ for coating and $a = m$ for matrix. Correspondingly, the stress fields in the coating and the matrix are given by:

$$\sigma_{rr}^{(a)} = 2G_i \left\{ B_1^{(a)} \frac{1+\nu_i}{1-2\nu_i} - 2B_2^{(a)} \frac{R_i^3}{r^3} + \frac{3\cos(2\theta)+1}{4}\left[-6\nu_i A_1^{(a)} \frac{r^2}{R_i^2} + 2A_2^{(a)} - 4(5-4\nu_i) A_3^{(a)} \frac{R_i^3}{r^3} + 12A_4^{(a)} \frac{R_i^5}{r^5}\right]\right\} \tag{13a}$$

$$\sigma_{r\theta}^{(a)} = -3G_i \sin(2\theta)\left[(7+2\nu_i) A_1^{(a)} \frac{r^2}{R_i^2} + A_2^{(a)} + 2(1+\nu_i) A_3^{(a)} \frac{R_i^3}{r^3} - 4A_4^{(a)} \frac{R_i^5}{r^5}\right], \tag{13b}$$

$$\sigma_{\theta\theta}^{(a)} = \frac{G_i}{2}\left\{\left[\frac{4(1+\nu_i)}{1-2\nu_i} B_1^{(a)} + \frac{4(1-\nu_i)}{1-2\nu_i}\frac{R_i^2}{r^2} B_2^{(a)}\right] - 6[5\nu_i + 7(2+\nu_i)\cos(2\theta)] A_1^{(a)} \frac{r^2}{R_i^2} - 2[-1+3\cos(2\theta)] A_2^{(a)} + 2(1-2\nu_i)[5+3\cos(2\theta)] A_3^{(a)} \frac{R_i^3}{r^3} - [3+7\cos(2\theta)] A_4^{(a)} \frac{R_i^5}{r^5}\right\}, \tag{13c}$$

where, again, $a = c$ for coating and $a = m$ for matrix, and $A_1^{(a)}$, $A_2^{(a)}$, $A_3^{(a)}$, $A_4^{(a)}$ and $B_1^{(a)}$, $B_2^{(a)}$ are coefficients to be determined from boundary conditions. Note that surface tension is involved in the boundary condition of Eq. (7), so it will affect the both the displacement and stress fields; also, with Eq. (3), the solutions are affected by the liquid compressibility.

The coefficients in Eq. (13) are determined in Supplementary Material S1, and their values are calculated by the software Mathematica 9. In Supplementary Material S2, we demonstrate that the solution of coated liquid inclusions with surface tension reduces to existing solutions in appropriate limits, including the solution of Chen et al. [28] for coated compressible liquid inclusions without surface effects, i.e., $\gamma = 0$, the solution of Style et al. [30] for incompressible liquid inclusion with surface effects, i.e., $G_c = G_m$, $\nu_c = \nu_m$, $R_c/R_i = 1$ and $K_i \to \infty$, and the solution of Chen et al. [3] for compressible liquid inclusion without surface effects, i.e., $G_c = G_m$, $\nu_c = \nu_m$, $R_c/R_i = 1$ and $\gamma = 0$.

3.2 Volumetric strain of the inclusion

To demonstrate the tuning role of the coating, it is necessary to clarify which behavior of the compressible liquid inclusion is the most important and needs to be tuned. As most of the coated inclusions in concern are cells at micro-millimeter scale, we need to identify the mechanical behaviors of cells that have significant influences on their physiological process. Recently, strong experimental evidences suggest that cell volume has important influence on cell physiological process [31–33]. On one hand, cell volume changes over the course of cell life cycle, increasing as cell plasma membrane grows and the amount of protein, DNA, and other intracellular material increases [34]. On the other hand, cell volume can also change on a much more rapid time scale, for example, when a cell deforms under external osmotic pressure: in this case, cell volume changes as a result of fluid transportation through cell membrane [35]. This causes increased concentration of intracellular material and molecular crowding [36, 37], causing numerous important consequences such as increase in stiffness [38], folding and transport of proteins [39], and condensation of chromatin [40].

In the following, for the coated liquid inclusion of Fig. 1, we focus on changes in its volumetric strain $\Delta V/V_0$ and pressure p. Note that, when a far field load is applied, the spherical liquid inclusion becomes an ellipsoid so that its linearized volumetric strain can be written as:

$$\frac{1}{\varepsilon^\infty}\frac{\Delta V}{V_0} = \frac{1}{\varepsilon^\infty R_i}\Big[u_r^{(c)}(r = R_i, \theta = 0) + u_r^{(c)}\Big(r = R_i, \theta = \frac{\pi}{2}\Big) + u_r^{(c)}\Big(r = R_i, \theta = \frac{\pi}{2}\Big). \tag{14}$$

Substituting the solution of Eq. (12) into Eq. (14) yields:

$$\frac{1}{\varepsilon^\infty}\frac{\Delta V}{V_0} = \frac{18\alpha^3 G_c G_m(1-\nu_c)(1-\nu_m)}{3\big(4G_m + 3K_i - 2\frac{\gamma}{R}\big)G_c(1-\nu_c) + \big(\alpha^3-1\big)\big(4G_c + 3K_i - 2\frac{\gamma}{R}\big)[2(1-2\nu_c)G_m + G_c(1+\nu_c)]}, \tag{15}$$

where $\alpha = R_c/R_i$. Note that $\frac{1}{\varepsilon^\infty}\frac{\Delta V}{V_0} > 0$, implying that the volume of the liquid inclusion increases when the far field load is stretch and decreases when the far field load is compression. In the limit when $R_c/R_i = 1$ and $\gamma = 0$, the volumetric strain of the no coating case is obtained:

$$\frac{1}{\varepsilon^\infty}\left(\frac{\Delta V}{V_0}\right)_0 = \frac{6G_m(1-\nu_m)}{4G_m + 3K_i}. \tag{16}$$

This coincides with the existing result [3] for the case of $\gamma = 0$ (no surface tension).

Finally, the tuning role of coating on the volumetric strain of the liquid inclusion can be explicitly described by:

$$\frac{1}{\varepsilon^\infty}\frac{\Delta V}{V_0} - \frac{1}{\varepsilon^\infty}\left(\frac{\Delta V}{V_0}\right)_0 = \frac{12\big(\alpha^3-1\big)(G_c - G_m)\Big[\Big(3K_i - \frac{2\gamma}{R}\Big)(1-2\nu_c) - 2G_c(1+\nu_c)\Big]G_m(1-\nu_m)}{(4G_m + 3K_i - \frac{2\gamma}{R})\Big\{3\Big(4G_m + 3K_i - \frac{2\gamma}{R}\Big)G_c(1-\nu_c) + \big(\alpha^3-1\big)\Big(4G_c + 3K_i - \frac{2\gamma}{R}\Big)[2G_m(1-2\nu_c) + G_c(1+\nu_c)]\Big\}}. \tag{17}$$

With Eq. (17), a positive difference means that the volumetric strain of the liquid inclusion is amplified by the coating. In contrast, the volumetric strain of the inclusion is attenuated by the coating when the difference of Eq. (17) is negative.

To determine the sign of the difference Eq. (17), we make use the bulk modulus of the coating

$$G_c = \frac{3K_c(1-2\nu_c)}{2(1+\nu_c)}, \tag{18}$$

and rewrite the difference as:

$$\frac{1}{\varepsilon^{\infty}}\frac{\Delta V}{V_0} - \frac{1}{\varepsilon^{\infty}}\left(\frac{\Delta V}{V_0}\right)_0 = \frac{12\left(\alpha^3-1\right)(G_c-G_m)\left(3K_i - \frac{2\gamma}{R} - 3K_c\right)G_m(1-2\nu_c)(1-\nu_m)}{(4G_m+3K_i-\frac{2\gamma}{R})\left\{3\left(4G_m+3K_i-\frac{2\gamma}{R}\right)G_c(1-\nu_c)+\left(\alpha^3-1\right)\left(4G_c+3K_i-\frac{2\gamma}{R}\right)[2G_m(1-2\nu_c)+G_c(1+\nu_c)]\right\}}. \tag{19}$$

to quantify the sensitivity of liquid volumetric strain to far-field strain. A larger value of $\frac{1}{\varepsilon^{\infty}}\frac{\Delta V}{V_0}$ implies that the inclusion volumetric strain is more sensitive to the far-field strain. The

As the denominator of the right hand side is always positive, the sign of Eq. (19) depends on the sign of $G_c - G_m$ and $K_i - \frac{2\gamma}{3R} - K_c$. Thus, the tuning role of the coating can be designed by tailoring its stiffness (relative to both matrix and inclusion) and thickness (relative to inclusion) as well as surface tension.

Intuitively, let the effective bulk modulus of the liquid inclusion be represented by $K_i - \frac{2\gamma}{3R}$. Then a mechanical signal is amplified by the coating when the stiffness variation from the matrix to the inclusion is monotonic (either increasing or decreasing). Alternatively, the mechanical signal is attenuated by the coating when stiffness from the matrix to the inclusion is non-monotonic, i.e., the coating exhibits a stiffness that is either greater or smaller than both the inclusion and the matrix.

4 Results

Because the Poisson ratio of common biomaterials and tissues falls within the range of 0.3–0.5 [41–43], we choose $\nu_c = 0.35$ and $\nu_m = 0.35$ in the following.

4.1 Influence of coating on volumetric strain of inclusion

Under far field uniaxial loading, the predicted effects of coating modulus and thickness on inclusion volumetric strain are displayed in Fig. 2. The volumetric strain increases first and then decreases with increasing shear modulus of the coating, as shown in Fig. 2a. In addition, when the liquid bulk modulus is smaller than the matrix shear modulus (e.g., $K_i/G_m = 0.1$), the influence of surface tension on inclusion volumetric strain is obvious. However, when the liquid bulk modulus is equal to or larger than the matrix shear modulus (e.g., $K_i/G_m = 1$ or $K_i/G_m = 10$), the influence of surface tension on volumetric strain is basically negligible. Note that, in Fig. 2a, we used a dimensionless volumetric strain $\frac{1}{\varepsilon^{\infty}}\frac{\Delta V}{V_0}$ case of no coating ($G_c = G_m$, $\nu_c = \nu_m$ and $R_c = R_i$) means the coating and the matrix are the same material and hence the coating effect will disappear. The results of Fig. 2a show that the inclusion volume is insensitive to the far field load when the shear modulus of the coating is much greater or smaller than the matrix, as the value of $\frac{1}{\varepsilon^{\infty}}\frac{\Delta V}{V_0}$ is vanishingly small. In contrast, when the shear modulus of the coating has a magnitude similar to that the matrix, the inclusion volumetric strain may be considerably amplified by the coating compared with the case of no coating (i.e., $G_c/G_m = 1$), as shown in Fig. 2a.

In Fig. 2b, the case of no coating means $R_c/R_i = 1$, i.e., when the thickness of the coating is zero. The intersection point of the solid line at $R_c/R_i = 1$ corresponds to the volumetric strain for the case of no coating with surface effect, while the intersection point of the dotted line at $R_c/R_i = 1$ corresponds to the volumetric strain for the case of no coating without surface effect. The lines below the intersection point mean that the coating attenuates the volumetric strain of the inclusion, that is, the inclusion volumetric strain is smaller than the case of no coating, regardless of surface effect. And this occurs when the coating is either softer or stiffer than both the matrix and the inclusion, thus satisfying $(G_c - G_m)\left(K_i - \frac{2\gamma}{3R} - K_c\right) < 0$. In sharp contrast, the lines above intersection point mean that the presence of a coating amplifies the volumetric strain of the inclusion: that is, regardless of surface effect, the inclusion volumetric strain is larger than the case of no coating. This occurs when a continuous stiffness gradient forms from the matrix via the coating to the inclusion, satisfying $(G_c - G_m)\left(K_i - \frac{2\gamma}{3R} - K_c\right) > 0$. We also observe that, in all the cases considered, the inclusion volume response $\frac{1}{\varepsilon^{\infty}}\frac{\Delta V}{V_0}$ converges to a limit value when the coating thickness is sufficiently large (i.e., $R_c/R_i \geq 3$). When the coating has a moderately large thickness (i.e., $1 \leq R_c/R_i \leq 2$), its influence on the inclusion volume response is significant.

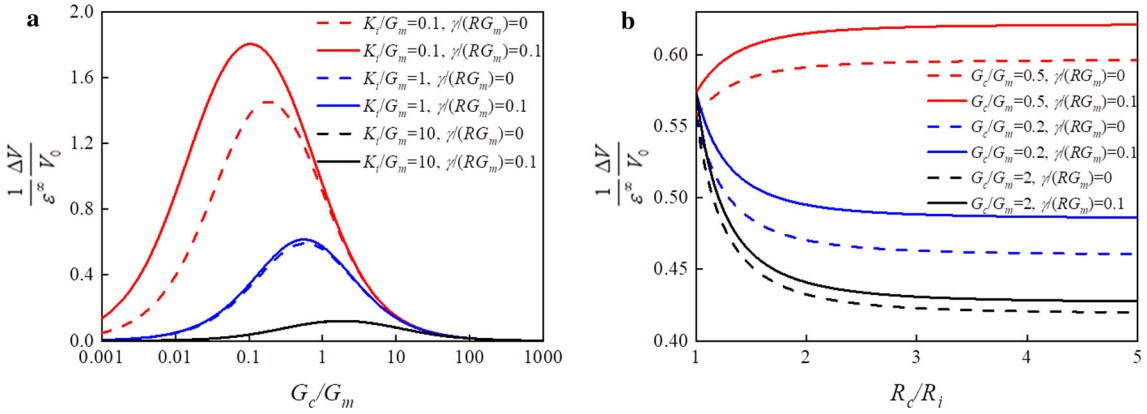

Fig. 2 Effect of modulus and thickness of the coating on volumetric strain of the inclusion. **a** Inclusion volumetric strain $\frac{1}{\varepsilon^\infty}\frac{\Delta V}{V_0}$ plotted as a function of the relative shear modulus G_c/G_m of the coating, with $R_c/R_i = 2$, $\nu_m = \nu_c = 0.35$. Different colored lines represent different relative liquid compressibility K_i/G_m. Dotted lines represent the case without surface tension (e.g., $\gamma/(RG_m) = 0$), and solid lines represent the case with surface tension (e.g., $\gamma/(RG_m) = 0.1$). **b** Inclusion volumetric strain $\frac{1}{\varepsilon^\infty}\frac{\Delta V}{V_0}$ is plotted as a function of the relative thickness R_c/R_i of the coating, with $K_i/G_m = 1$, $\nu_m = \nu_c = 0.35$. Different colored lines represent different values of the relative shear modulus of the coating. Dotted lines correspond to the case without surface tension, while solid lines correspond to the case with surface tension

4.2 Influence of liquid compressibility on deformation of inclusion

Under far field uniaxial loading, the displacement of point A at inclusion-coating interface (Fig. 1) decreases with increasing liquid bulk modulus, as shown in Fig. 3. As surface tension is increased, this displacement also decreases, which means the presence of surface tension tends to block the deformation of point A. In the limit $K_i/G_m \to \infty$ (i.e., the liquid inclusion becomes incompressible), the present result tends to that obtained by Mancarella et al. [27]. In the limit $\gamma/(RG_m) \to 0$ (i.e., surface effect is absent), the present result reduces to that of Chen et al. [3].

Figure 4 plots the inclusion volumetric strain $\frac{1}{\varepsilon^\infty}\frac{\Delta V}{V_0}$ as a function of dimensionless liquid compressibility K_i/G_m for selected values of relative shear modulus G_c/G_m and surface tension. The volumetric strain gradually decreases with the increase of liquid compressibility, and the change is small when the compressibility is relatively small or large. In the limit when the liquid inclusion tends to incompressible, the volumetric strain becomes negligibly small as expected. However, the change becomes sharp when the compressibility is moderately large. From Fig. 4, it can also be seen that when the shear modulus of the coating is smaller than that of the matrix, surface tension has a greater influence on volumetric strain; in contrast, when the modulus of the coating is larger than that of the matrix, the influence of surface tension on volumetric strain can be neglected.

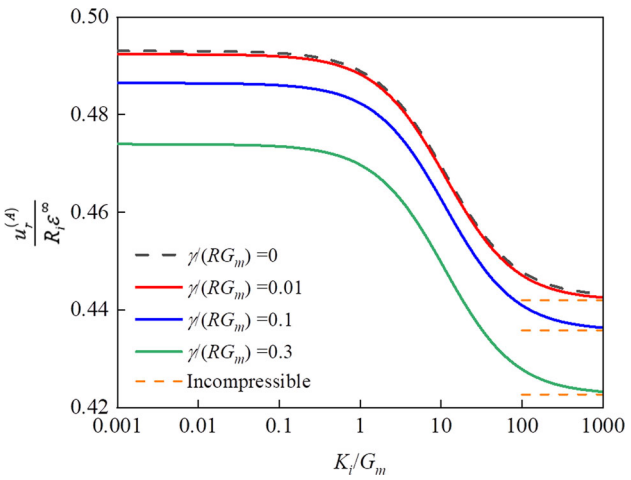

Fig. 3 Effect of liquid compressibility on radial displacement of the inclusion. The x-axis is the dimensionless liquid compressibility K_i/G_m, and the y-axis is the radial displacement of the inclusion at point A $u_r^{(A)}/(R_i\varepsilon^\infty)$ under uniaxial tension. Different colored solid lines represent different values of surface tension. The black dotted line shows the classic result without surface tension [3]. Orange dotted horizontal lines on the right indicate surface tension effects on incompressible liquid inclusion [27]. When surface tension tends to zero, the solid red line is basically coincident with the dotted black line. When the compressibility of liquid tends to infinity, the results reduce to those obtained Style et al. [27]

5 Discussion

5.1 Strain attenuation of cancer cell

Fibrous tissue is typically present around a cancer cell (Fig. 5a), which can be considered as a coating that is wrapped in healthy tissue. To simplify the model, the cancer

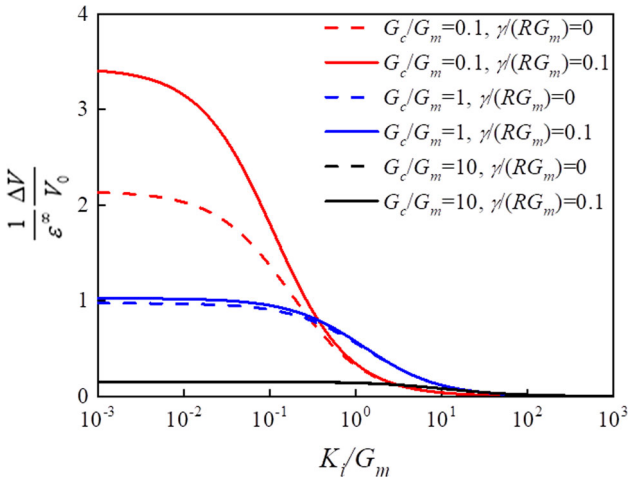

Fig. 4 Effect of the compressibility of liquid inclusion on its volumetric strain. The x-axis is the dimensionless liquid compressibility K_i/G_m, and the y-axis is the volumetric strain $\frac{1}{\varepsilon^\infty}\frac{\Delta V}{V_0}$. Different colored lines represent different dimensionless values of relative shear modulus G_c/G_m. Dotted lines represent the case without surface tension (e.g., $\gamma/(RG_m) = 0$), and solid lines represent the case with surface tension (e.g.,$\gamma/(RG_m) = 0.1$). Here $R_c/R_i = 2$, $\nu_m = \nu_c = 0.35$

Table 1 Range of mechanical properties for liver cancer cell model

Symbol	Variable	Range of data	Baseline value
E_m(kPa)	Young's modulus of the liver normal tissue	0.3–0.6 [48]	0.6
E_c(kPa)	Young's modulus of the liver cancer tissue	1.6–20 [48, 49]	20
E_i(kPa)	Young's modulus of the liver cancer cell	Fibroblasts ~ 1 [8]	1
R_i(μm)	Radius of the f the mouse embryonic stem cells	5 [50]	5
γ(N/m)	surface energy density on the cell surface	0–0.05 [51]	0.01

cell is treated as a spherical liquid inclusion, the fibrous tissue as a spherical coating, and the normal tissue as an infinite elastic matrix, as shown schematically in Fig. 5b. Relevant parameters chosen for the model of coated cancer cell are listed in Table 1, including a basal set of fixed values as well as reasonable ranges of variation and sources of data. The Young's modulus of normal and pathological liver tissue are 0.6 kPa and 20 kPa, and the Young's modulus of cancer cell is 1 kPa (Table 1). The radius of the cell is $R_i = 5$ μm and surface energy density of the interface is $\gamma = 0.01$ N/m (Table 1). We assume that the Poisson ratios of the cancer cell, healthy tissue and fibrous tissue are all fixed at 0.4. Using these data, we quantified the effect of far-field strain on the volumetric strain of liver cancer cell with or without a coating, as shown in Fig. 5c.

We can see from Fig. 5c that, in the presence of surface tension, the volumetric strain of cancer cell with coating is about a third of that of cancer cell without coating. Further, the volumetric strain of the cancer cell increases as surface effect is increased. This reflects the coating around the cancer cell would prevent the cell from receiving external mechanical signals (e.g., signals transmitted via surrounding environment). Note that surface tension attenuates the volumetric strain of the inclusion by decreasing its effective bulk modulus $K_i - \frac{2\gamma}{3R}$. The mechanical properties of fibrous tissue (i.e., coating in the present study) in specific organs contribute to the preferential migration, attachment, survival and proliferation of cancer cells [9, 44–46]. The coating-induced strain attenuation may be the mechanism underlying such behaviors of cancer cells.

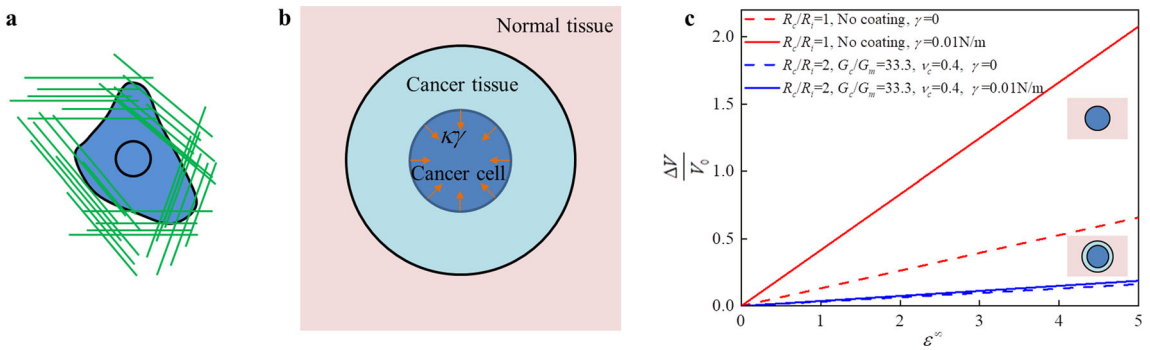

Fig. 5 Effect of far-field strain on volumetric strain of liver cancer cells**. a** Schematic illustration of cancer cell and its surrounding. **b** Effective model of cancer cell with coating embedded in tissue. **c** Effect of far-field strain on volumetric strain of liver cancer cell. The x-axis is the far-field strain ε^∞, which is the tissue strain, and the y-axis is the volumetric strain of the cell. Different colored lines represent different results obtained with different theories: red lines represent the classical inclusion theory without coating, and blue lines represent the present theory considering coating. Here, $R = 10$ μm is assumed in our coating model

5.2 Strain amplification of osteocyte in bone

Osteocytes exist in bone and are cells that can specifically secrete a variety of bioactive substances to regulate and influence the formation and reconstruction of the bone. Existing studies have shown that osteocytes experience some form of strain amplification in bone, because the strains that elicit an osteogenic response would damage the extracellular matrix (bone) [6]. With reference to Fig. 6, we simplify the osteocytes model in order to explain strain amplification of osteocytes using our model of coated liquid inclusions. From the scanning electron microscopy (SEM) image of Fig. 6a [47], we can see that osteocyte has numerous protruding parts, i.e., the cell processes. Further, the osteocyte and its processes are surrounded by a layer of PCM and, outside the PCM, there exists a layer of ECM composed of bone. Based upon these observations, we simplify the osteocyte model as an inclusion having lots of cell processes embedded in the PCM, as shown schematically in Fig. 6b: the cell is considered as a spherical compressible liquid inclusion, and the processes are periodically distributed around the cell. The cell and its processes are coated by the PCM, which is coated by the ECM. As the cell scale is at the micron level, surface tension at the interface between the cell and PCM should be considered. Further, for simplicity, we assume that the cell processes, the PCM and part of the ECM in the outside of the cell body can be homogenized as an effective coating wrapping around the cell, and the effective coating is coated by infinite ECM, as shown in Fig. 6c.

To analyze the coated inclusion model of osteocytes, we first need to determine the modulus and Poisson ratio of the effective coating. In the present study, the effective modulus and Poisson ratio of the idealized coating shown in Fig. 6c may be estimated by volume fraction, as:

$$G_c = \phi_p G_p + \phi_{PCM} G_{PCM} + \phi_{ECM} G_{ECM}, \tag{20}$$

where G_c is the effective shear modulus of the coating, ϕ_p, ϕ_{PCM} and ϕ_{ECM} are the volume fractions of the cell processes, the PCM and the ECM, and G_p, G_{PCM} and G_{ECM} are the shear modulus of the cell processes, the PCM and the ECM, respectively. Using Eq. (20), the data from Table 2 and assuming that $\phi_p = 0.1$, ϕ_{PCM}=0.5, ϕ_{ECM}=0.4 and $R_i = 5$ μm according to the 3D reconstruction image of osteocyte [52], we calculated the effective shear modulus of its coating to be approximately $G_c = 0.4G_m$. Similarly, we estimated the effective Poisson ratio of the coating, ν_c, to be 0.38. In passing, it should be pointed out that, as the modulus of the matrix (bone) is too large, the effect of surface tension on the volumetric strain of the cell can be neglected. Consequently, we only considered two cases: the model with coating and the model without coating.

In Fig. 7, we plotted the volumetric strain $\frac{1}{\varepsilon^\infty}\frac{\Delta V}{V_0}$ of the osteocyte as a function of far-field strain ε^∞ (i.e., bone strain) for the two cases considered. According to Verbruggen et al. [6], disuse bone resorption begins at a bone strain level

Table 2 Range of mechanical properties for osteocyte cell model

Symbol	Variable	Range of data	Baseline value
E_c,E_p (kPa)	Young's modulus of the osteocyte and processes	2.4–4.7 [53]	4.47
ν_c,ν_p	Poisson's ratio of the osteocyte and processes	0.3–0.496 [54]	0.3
E_{PCM}(kPa)	Young's modulus of the pericellular matrix	40–70 [55]	40
ν_{PCM}	Poisson's ratio of the pericellular matrix	0.4 [6]	0.4
E_{ECM}(GPa)	Young's modulus of the extracellular matrix	13.6–25.2 [56]	16
ν_{ECM}	Poisson's ratio of the extracellular matrix	0.25–0.43 [56]	0.38

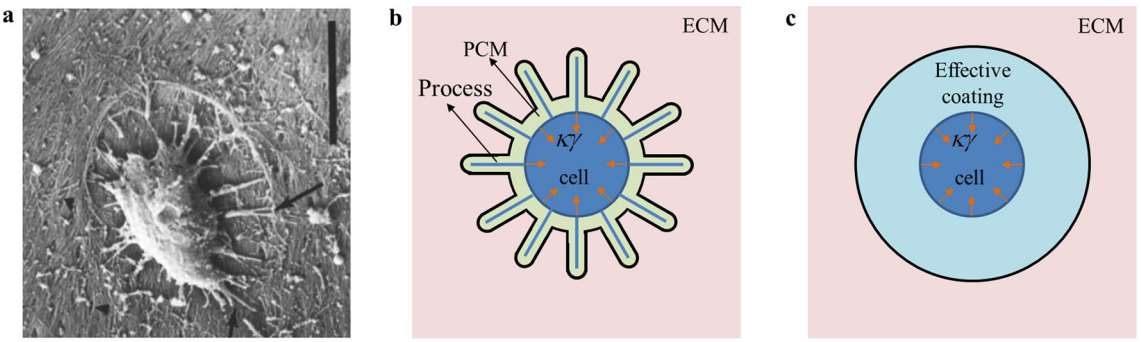

Fig. 6 SEM image and schematic illustration of osteocytes. **a** SEM image of osteocyte (× 2500) [47]. The arrow is the cell process. The bar is 10 μm, tilt 30°. **b** Schematic of osteocyte. **c** Effective model of osteocyte

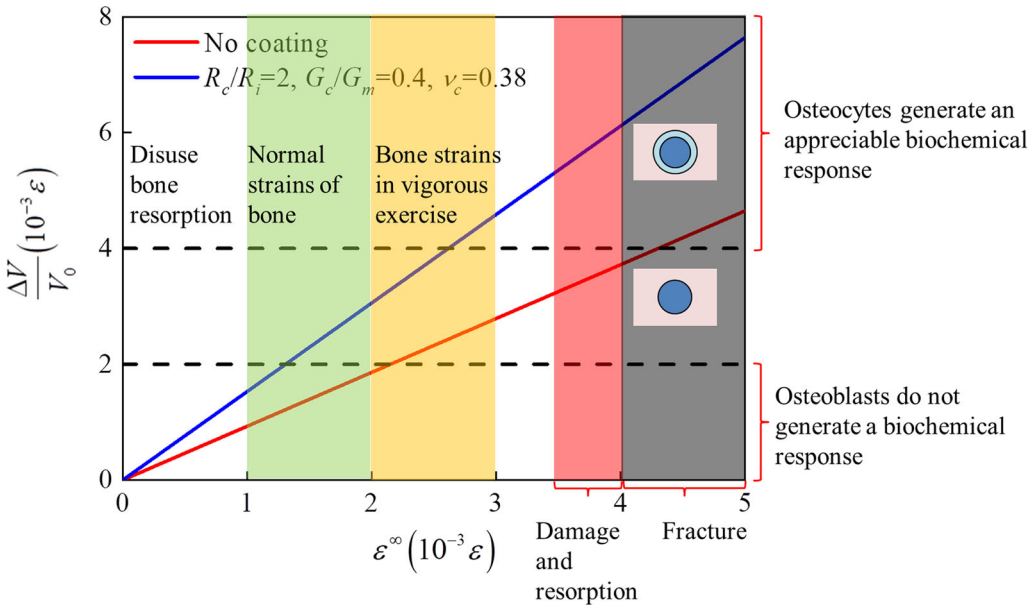

Fig. 7 Effect of far-field strain on osteocytes volumetric strain. The x-axis is the far-field strain ε^{∞}, which is the bone strain, and the y-axis is the volumetric strain $\frac{1}{\varepsilon^{\infty}}\frac{\Delta V}{V_0}$ of the cell. Different colored lines represent different cell models. The red line is the classical inclusion theory without coating, and the blue line is the theory considering coating and surface tension. The different colored areas on the x-axis indicate the strain range of the bone during different intensities of activity. The first black dotted line represents that osteocytes cultured in vitro do not generate a biochemical response when the strain is less than the value. And an appreciable response occurs when the strain is more than the value of the second black dotted line. Here $R = 5$ μm in our coating model

less than $10^{-3}\varepsilon$; the bones routinely experience mechanical strains between $10^{-3}\varepsilon$ and $2 \times 10^{-3}\varepsilon$; vigorous exercise can generate strains up to $3 \times 10^{-3}\varepsilon$; a strain more than $3.5 \times 10^{-3}\varepsilon$ results in bone damage and absorption; and a strain more than $4 \times 10^{-3}\varepsilon$ results in bone fracture (Fig. 7). When the volumetric strain is small (i.e., below the first flash line), osteocytes cultured in vitro do not generate a biochemical response, but an appreciable response occurs when the volumetric strain becomes larger (i.e., above the second flash line). In the presence of a uniaxial load at far field, the volumetric strain response of osteocyte with coating (blue line) is larger than that without coating (red line): that is, the coating of osteocyte causes strain amplification. Such strain amplification of osteocytes is of significance for the mechanobiological sensation of bone. For typical instance, osteocytes with coating cangenerate an appreciable response during vigorous exercise (e.g., running). In sharp contrast, for osteocytes without coating, there is no appreciable response to such loading until the bone is fractured, as shown in Fig. 7.

6 Conclusions

We have established a mechanical model for a coated compressible spherical liquid inclusion embedded in infinite elastic matrix and solved it analytically, with surface tension effects accounted for. We found that, in the presence of far field loading, surface tension can decrease the effective bulk modulus of the liquid inclusion, which leads to an increase of its volumetric strain compared with the case without surface tension. Further, we found that whether the volumetric strain of liquid inclusion will be amplified or attenuated depends mainly on liquid bulk modulus, surface tension, coating shear modulus, and matrix bulk modulus. Relative to the case without coating, the volumetric strain is amplified by the coating if there is a monotonic variation of stiffness from the matrix via the coating to the inclusion. In the opposite, if there is a non-monotonic stiffness variation from the matrix, coating to inclusion, the volumetric strain is attenuated by the coating. Besides, the model was then used to investigate two common examples of coated inclusions in biological bodies, i.e., cancer cells and osteocytes. Our theoretical results are helpful for understanding the biological significance of amplification and attenuation mechanisms of these cells.

In addition to explaining the amplification and attenuation of far-field strain, our model could explain that the ECM locally stiffened by a cancer cell can amplify the signal a cell generates [57]. However, the counterpart of this problem remains unclear—how this stiffened region influences the capability of a cell to sense the mechanical signals in its "neighborhood". In the simplest manner, this stiffened region could be regarded as a layer of stiff coating, thus enabling a non-monotonic stiffness variation from the matrix, coating to inclusion. Our results then suggest that this coating could

amplify the signal generated by a cell, which is consistent with experimental results [57].

In most of the previous works regarding cell mechanosignaling, the influence of a cell on the extracellular matrix is treated as a force boundary [58], or a displacement boundary [57, 59]. However, the elastic response of what is inside the cell should play a role. First, the contractility of cell comes from actin myosin contraction. Forming a layer below the cell membrane, the actin contracts not only the ECM, but also the inner part of cell. Second, it has been shown that it is actually very crowded inside a cell [60], including high amount of actin, microtubules, intermediate filaments and etc. Our model suggests that cell elasticity plays a key role in determining whether or not the signal is amplified. The model also shows that the influence of this elasticity could be treated as an equivalent actin contractility. The actin contractility can be regarded as cortical stress [61], which can be regarded as a special type of surface tension. Besides, our results suggest that the bulk modulus of the liquid inclusion (cell) and surface tension can be interconverted. On one hand, the bulk modulus and the surface tension can be regarded as the effective bulk modulus; on the other hand, the bulk modulus could be regarded as a special surface tension, which can be treated as a force boundary.

Acknowledgements This work was financially supported by the National Natural Science Foundation of China (Grants 12032010, 11532009, and 11902155), the Natural Science Foundation of Jiangsu Province (Grant BK20190382), the foundation of "Jiangsu Provincial Key Laboratory of Bionic Functional Materials", the Foundation for the Priority Academic Program Development of Jiangsu Higher Education Institutions.

References

1. Krishnan, R., Park, C.Y., Lin, Y.C., et al.: Reinforcement versus fluidization in cytoskeletal mechanoresponsiveness. PLoS ONE **4**(5), e5486 (2009)
2. Chen, X., He, W., Liu, S., et al.: Volumetric response of an ellipsoidal liquid inclusion: implications for cell mechanobiology. Acta. Mech. Sin. **35**(2), 338–342 (2019)
3. Chen, X., Li, M., Yang, M., et al.: The elastic fields of a compressible liquid inclusion. Extreme Mech. Lett. **22**, 122–130 (2018)
4. Hagan, M.L., Yu, K., Zhu, J., et al.: Decreased pericellular matrix production and selection for enhanced cell membrane repair may impair osteocyte responses to mechanical loading in the aging skeleton. Aging Cell **19**(1), e13056 (2020)
5. Khoshgoftar, M., Torzilli, P.A., Maher, S.A.: Influence of the pericellular and extracellular matrix structural properties on chondrocyte mechanics. J. Orthop. Res. **36**(2), 721–729 (2018)
6. Verbruggen, S.W., Vaughan, T.J., Mcnamara, L.M.: Strain amplification in bone mechanobiology: a computational investigation of the in vivo mechanics of osteocytes. J. R. Soc. Interface **9**(75), 2735–2744 (2012)
7. Wang, L., Dong, J., Xian, C.J.: Computational modeling of bone cells and their biomechanical behaviors in responses to mechanical stimuli. Crit. Rev. Eukaryot. Gene Expr. **29**(1), 51–67 (2019)
8. Yu, H., Mouw, J.K., Weaver, V.M.: Forcing form and function: biomechanical regulation of tumor evolution. Trends Cell Biol. **21**(1), 47–56 (2011)
9. Kumar, S., Weaver, V.M.: Mechanics, malignancy, and metastasis: the force journey of a tumor cell. Cancer Metastasis Rev. **28**(1–2), 113–127 (2009)
10. Eshelby, J.D.: The determination of the elastic field of an ellipsoidal inclusion, and related problems. Pro. Roy. Soc. A **241**(1226), 376–396 (1957)
11. Walpole, L.J.: A coated inclusion in an elastic medium. Math. Proc. Cambridge Philos. Soc. **83**(3), 495–506 (1978)
12. Jayaraman, K., Reifsnider, K.L.: Residual stresses in a composite with continuously varying Young's modulus in the fiber/matrix interphase. J. Compos. Mater. **26**(6), 770–791 (1992)
13. Vörös, G., Pukánszky, B.: Effect of a soft interlayer with changing properties on the stress distribution around inclusions and yielding of composites. Compos. A **32**(3), 343–352 (2001)
14. Duan, H.L., Wang, J., Huang, Z.P., et al.: Stress fields of a spheroidal inhomogeneity with an interphase in an infinite medium under remote loadings. Proc R Soc A **461**(2056), 1055–1080 (2005)
15. Bertoldi, K., Bigoni, D., Drugan, W.J.: Structural interfaces in linear elasticity. Part II: Effective properties and neutrality. J. Mech. Phys. Solids **55**(1), 35–63 (2007)
16. Yi, M.W., Huang, Z.P., Yan, Z., et al.: Effective moduli of particle-filled composite with inhomogeneous interphase: Part I–bounds. Compos. Sci. Technol. **64**(9), 1345–1351 (2004)
17. Yan, Z., Wang, J., Yi, M.W., et al.: Effective moduli of particle-filled composite with inhomogeneous interphase: Part II–mapping method and evaluation. Compos. Sci. Technol. **64**(9), 1353–1362 (2004)
18. Hashin, Z.: Thin interphase/imperfect interface in elasticity with application to coated fiber composites. J. Mech. Phys. Solids **50**(12), 2509–2537 (2002)
19. Bai, S.L., Wang, G.T., Hiver, J.M., et al.: Microstructures and mechanical properties of polypropylene/polyamide 6/polyethelene-octene elastomer blends. Polymer **45**(9), 3063–3071 (2004)
20. Ostoja-Starzewski, M., Jasiuk, I., Wang, W., et al.: Composites with functionally graded interphases: mesocontinuum concept and effective transverse conductivity. Acta Mater. **44**(5), 2057–2066 (1996)
21. Wang, W., Jasiuk, I.: Effective elastic constants of particulate composites with inhomogeneous interphases. J. Compos. Mater. **32**(15), 1391–1424 (1998)
22. Christensen, R.M., Lo, K.H.: Solutions for effective shear properties in three phase sphere and cylinder models. J. Mech. Phys. Solids **27**(4), 315–330 (1979)
23. Mancarella, F., Wettlaufer, J.S.: Surface tension and a self-consistent theory of soft composite solids with elastic inclusions. Soft Matter **13**(5), 945–955 (2017)
24. Xiao, J., Xu, B.-X., Xu, Y., et al.: The generalized self-consistent micromechanics prediction of the magnetoelectroelastic properties of multi-coated nanocomposites with surface effect. Smart Mater. Struct. **28**(5), 055004 (2019)
25. Peng, C., Feng, J., Feiting, S., et al.: Modified two-phase micromechanical model and generalized self-consistent model for predicting dynamic modulus of asphalt concrete. Constr. Build. Mater. **201**, 33–41 (2019)
26. Lurie, S., Solyaev, Y., Shramko, K.: Comparison between the Mori-Tanaka and generalized self-consistent methods in the framework of anti-plane strain inclusion problem in strain gradient elasticity. Mech. Mater. **122**, 133–144 (2018)
27. Mancarella, F., Style, R.W., Wettlaufer, J.S.: Interfacial tension and a three-phase generalized self-consistent theory of non-dilute soft composite solids. Soft Matter **12**(10), 2744 (2016)

28. Chen, X., Li, M., Liu, S., et al.: Mechanics tuning of liquid inclusions via bio-coating. Extreme Mech. Lett. **2020**, 101049 (2020)
29. Shafiro, B., Kachanov, M.: Materials with fluid-filled pores of various shapes: Effective elastic properties and fluid pressure polarization. Int. J. Solids Struct. **34**(27), 3517–3540 (1997)
30. Style, R.W., Wettlaufer, J.S., Dufresne, E.R.: Surface tension and the mechanics of liquid inclusions in compliant solids. Soft Matter **11**(4), 672–679 (2015)
31. Guo, M., Pegoraro, A.F., Mao, A., et al.: Cell volume change through water efflux impacts cell stiffness and stem cell fate. Pro. Natl. Acad. Sci. USA **114**(41), 201705179 (2017)
32. Wang, M., Yang, Y., Han, L., et al.: Cell mechanical microenvironment for cell volume regulation. J. Cell. Physiol. **235**(5), 4070–4081 (2020)
33. Liu, A., Yu, T., Young, K., et al.: Cell mechanical and physiological behavior in the regime of rapid mechanical compressions that lead to cell volume change. Small **16**(2), 1903857 (2020)
34. Amit, T., Ran, K., Lebleu, V.S., et al.: Cell growth and size homeostasis in proliferating animal cells. Science **325**(5937), 167–171 (2009)
35. Hui, T.H., Zhou, Z.L., Qian, J., et al.: Volumetric deformation of live cells induced by pressure-activated cross-membrane ion transport. Phys. Rev. Lett. **113**(11), 118101 (2014)
36. Badowski, C., Iskander, A., Gaspar, D., et al.: Molecular crowding–(in cell culture). Cell Eng. Regener. **2020**, 483–509 (2020)
37. Watanabe, C., Yanagisawa, M.: Unique phase behavior in cell size space: synergistic effect of molecular crowding and confinement. Biophys. Rev. **12**(2), 385 (2020)
38. Liao, H.S., Wen, P.J., Wu, L.G., et al.: Effect of osmotic pressure on cellular stiffness as evaluated through force mapping measurements. J. Biomech. Eng. **140**(5), 054502 (2018)
39. Oh, D., Zidovska, A., Xu, Y., et al.: Development of time-integrated multipoint moment analysis for spatially resolved fluctuation spectroscopy with high time resolution. Biophys. J. **101**(6), 1546–1554 (2011)
40. Jerome, I., Joe, S., Rui, P., et al.: Osmotic challenge drives rapid and reversible chromatin condensation in chondrocytes. Biophys. J. **104**(4), 759–769 (2013)
41. Charras, G.T., Horton, M.A.: Determination of cellular strains by combined atomic force microscopy and finite element modeling. Biophys. J. **83**(2), 858–879 (2002)
42. Kelly, G.M., Kilpatrick, J.I., Van Es, M.H., et al.: Bone cell elasticity and morphology changes during the cell cycle. J. Biomech. **44**(8), 1484–1490 (2011)
43. Rubiano, A., Galitz, C., Simmons, C.S.: Mechanical characterization by mesoscale indentation: advantages and pitfalls for tissue and scaffolds. Tissue Eng. Part C **25**(10), 619–629 (2019)
44. Kostic, A., Lynch, C.D., Sheetz, M.P.: Differential matrix rigidity response in breast cancer cell lines correlates with the tissue tropism. PLoS ONE **4**(7), e6361 (2009)
45. Lam, W.A., Cao, L., Umesh, V., et al.: Extracellular matrix rigidity modulates neuroblastoma cell differentiation and N-myc expression. Mol. Cancer **9**(1), 35 (2010)
46. Pathi, S.P., Kowalczewski, C., Tadipatri, R., et al.: A novel 3-D mineralized tumor model to study breast cancer bone metastasis. PLoS ONE **5**(1), e8849 (2010)
47. Menton, D., Simmons, D., Chang, S.L., et al.: From bone lining cell to osteocyte—an SEM study. Anatom. Record **209**(1), 29–39 (1984)
48. Wells, R.G.: The role of matrix stiffness in regulating cell behavior. Hepatology **47**(4), 1394–1400 (2008)
49. Yeh, W.-C., Li, P.-C., Jeng, Y.-M., et al.: Elastic modulus measurements of human liver and correlation with pathology. Ultrasound Med. Biol. **28**(4), 467–474 (2002)
50. Ladjal, H., Hanus, J.L., Pillarisetti, A., et al.: Atomic force microscopy-based single-cell indentation: experimentation and finite element simulation. in: International Conference on Intelligent Robots and Systems. St. Louis, MO (2009)
51. Ding, Y., Xu, G.-K., Wang, G.-F.: On the determination of elastic moduli of cells by AFM based indentation. Sci. Rep. **7**, 45575 (2017)
52. Sugawara, Y., Ando, R., Kamioka, H., et al.: The three-dimensional morphometry and cell–cell communication of the osteocyte network in chick and mouse embryonic calvaria. Calcif. Tissue Int. **88**(5), 416–424 (2011)
53. Sugawara, Y., Ando, R., Kamioka, H., et al.: The alteration of a mechanical property of bone cells during the process of changing from osteoblasts to osteocytes. Bone **43**(1), 19–24 (2008)
54. McCreadie, B.R., Hollister, S.J.: Strain concentrations surrounding an ellipsoid model of lacunae and osteocytes. Comput. Methods Biomech Bio Med. Eng. **1**(1), 61–68 (1997)
55. Guilak, F., Alexopoulos, L.G., Upton, M.L., et al.: The pericellular matrix as a transducer of biomechanical and biochemical signals in articular cartilage. Ann. N. Y. Acad. Sci. **1068**(1), 498–512 (2006)
56. Kato, N., Koshino, T., Saito, T., et al.: Estimation of Young's modulus in swine cortical bone using quantitative computed tomography. Bulletin. **57**(4), 183–186 (1998)
57. Han, Y.L., Ronceray, P., Xu, G., et al.: Cell contraction induces long-ranged stress stiffening in the extracellular matrix. Proc. Natl. Acad. Sci. **115**(16), 4075–4080 (2018)
58. Ronceray, P., Broedersz, C.P., Lenz, M.: Fiber networks amplify active stress. Proc. Natl. Acad. Sci. **113**(11), 2827–2832 (2016)
59. Ban, E., Wang, H., Franklin, J.M., et al.: Strong triaxial coupling and anomalous Poisson effect in collagen networks. Proc. Natl. Acad. Sci. **116**(14), 6790–6799 (2019)
60. Fletcher, D.A., Mullins, R.D.: Cell mechanics and the cytoskeleton. Nature **463**(7280), 485–492 (2010)
61. Jiang, H., Sun, S.X.: Cellular pressure and volume regulation and implications for cell mechanics. Biophys. J. **105**(3), 609–619 (2013)